ACS APPLIED ELECTRONIC MATERIALS

pubs.acs.org/acsaelm Article

Non-covalent Functionalization of Pristine and Defective WSe_2 by Electron Donor and Acceptor Molecules

Amine Slassi,* Adam Gali,* Jérôme Cornil, and Anton Pershin*

Cite This: ACS Appl. Electron. Mater. 2023, 5, 1660−1669 Read Online

ACCESS | Metrics & More | Article Recommendations | Supporting Information

ABSTRACT: Two-dimensional transition-metal dichalcogenide (2D-TMD) monolayers have recently attracted growing interest, thanks to their excellent optoelectronic properties, especially a moderate direct band gap in the visible spectral range and an extremely strong light−matter interaction. Herein, by means of density functional theory (DFT) and ab initio molecular dynamics (AIMD), we systematically investigate the chemical doping of the WSe_2 monolayer upon non-covalent attachment of electron donor and acceptor molecules, namely, fullerenes (C_{20}, C_{26}, and C_{60}), tetrathiafulvalene (TTF), 7,7,8,8-tetracyanoquinodimethane (TCNQ), and 2,3,5,6-tetrafluoro-7,7,8,8-tetracyanoquinodimethane (F_4-TCNQ). Our results confirm that the physisorbed molecules stack on WSe_2 via a weak van der Waals interaction; this precludes any significant damage in the basal-plane structure of the monolayer. In turn, the modifications in the carrier density in the WSe_2 monolayer due to organic dopants result in a change of the work function by up to 0.41 eV. By performing AIMD calculations, we show that the effect is more pronounced upon increasing the coverage density of physisorbed TTF and TCNQ molecules. The impact of Se-vacancy (V_{Se}) defects on the electronic properties of the WSe_2 monolayer and thermodynamic stability of physisorption (including the molecular density) is also considered. Interestingly, the molecules demonstrate an ability to modulate the degree of spatial localization of V_{Se} trap states. Moreover, the shift of the Fermi level upon molecular adsorption also enables further stabilization of charged defect states associated to a V_{Se} vacancy. The pronounced effect of molecular adsorption on the V_{Se} defect behavior in WSe_2 might open the door for potential engineering of defect states in 2D TMDs.

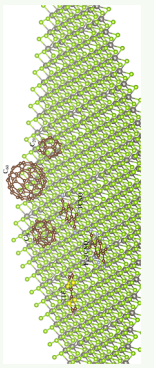

KEYWORDS: *WSe_2 monolayer, DFT, physisorption, selenium vacancy defect, thermodynamic stability*

1. INTRODUCTION

Two-dimensional (2D) layered transition-metal dichalcogenides (TMDs) with the chemical composition MX_2 (M = Mo and W; X = S and Se) have recently attracted tremendous attention, due to their unique electronic and optical properties, promising efficient utilization in high-performance optoelectronic devices, with targeted applications in catalysis,[1,2] energy storage,[3] photodetectors,[4] and flexible nanoelectronics.[5] In optoelectronics, the monolayer of molybdenum disulfide (MoS_2) is the most used TMD, due to its long history and excellent properties.[6−9] More recently, tungsten diselenide (WSe_2) has evolved as a rising star of the TMD family and has been successfully integrated in various technologies.[10,11] The WSe_2 monolayer exhibits a number of spectacular properties, starting with an efficient ambipolar charge transport.[12−15] Moreover, WSe_2 possesses a direct band gap of 1.6 eV in the visible spectral range, giving rise to a robust photoluminescence.[16]

In order to utilize the WSe_2 monolayer in high-performance devices, it is vital to modulate the charge carrier concentration.[17] To this end, chemical doping is an effective approach, applied to tune and control the electrical properties of 2D materials. In particular, molecular functionalization of the TMD surface represents a viable approach to induce either n- or p-type doping; moreover, this approach has the capability to modify the electronic properties without interfering with the basal-plane structure of a 2D material.[18−25] In such devices, doping is achieved through a charge transfer from the adsorbed molecules to the 2D materials (or vice versa). The effect is caused either by the difference in the chemical potentials of the two components or by an intrinsic molecular dipole, which acts as a local gate and induces a shift in the work function (WF).[19,20] Importantly, the atomic flatness and lack of dangling bonds on the surface of TMDs make the non-covalent interactions with molecules easy to activate and allow us to overcome the lattice matching requirements. For the WSe_2 monolayer, one interesting feature is that p-type doping can be easily achieved upon heterostructure stacking, with a proper adjustment of the relative positions of the conduction band minimum (CBM) and the valence band minimum (VBM); this is in contrast to MoS_2, where the n-type doping is prevalent.[26]

In recent years, various theoretical and experimental studies focused on the deposition of electron-donor and electron-acceptor molecules on top of TMD monolayers (mostly on

Received: December 14, 2022
Accepted: February 16, 2023
Published: February 28, 2023

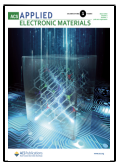

https://doi.org/10.1021/acsaelm.2c01718
ACS Appl. Electron. Mater. 2023, 5, 1660−1669

MoS_2), including MoS_2/TTF,[22,23] $MoSe_2$/TCNQ,[22,23] MoS_2/F_4-TCNQ,[21] MoS_2/TCNE (tetracyanoethylene),[22,23] MoS_2/C_{60},[27,28] MoS_2/C_{20},[27,28] MoS_2/C_{26},[28] WS_2/C_{60},[27] and WSe_2/C_{60}[29] heterostructures. By constructing the TMD/molecular stacks, these studies confirmed a significant modulation of the electronic structure and optical properties of TMDs upon molecular adsorption. For instance, the typical acceptor molecules (F_4-TCNQ and TCNQ) withdraw electrons from TMDs, while donor molecules yield an opposite effect. The electron redistribution gives rise to an interlayer dipole moment and to a respective increase/decrease in the work function depending on its orientation. Recently, Liu et al.[30] fabricated a memory device based on molecules/WSe_2 heterostructures, in which 2,3-dichloro-5,6-dicyano-1,4-benzoquinone (DDQ), TCNQ, F_4-TCNQ, TCNE, and TTF have been used. Moreover, even small molecules, commonly used for processing 2D materials during fabrication, are able to provide sizable modifications in the optoelectronic properties of MoS_2 and WSe_2 monolayers.[19]

On the other hand, a redistribution of the electron density at the hybrid surfaces represents a known strategy to modify the properties of deep defects.[31−33] For the TMDs, the defects such as chalcogen vacancies are of particular importance, since those are predominantly observed in TMD materials and are naturally formed during fabrication and operation processes.[31,34,35] The theoretical and experimental studies revealed that the chalcogen vacancies create new trap states and act as scattering centers, deteriorating the electron mobility.[36−38] Importantly, the strength of the scattering increases for higher charge states of the vacancy.[32] Several methods were suggested to heal this defect, including the passivation of defects in MoS_2 by substitutional oxygen doping of S-vacancy[33,39] or by covalently grafting molecules in the voids.[32,33] Another study suggested neutralizing the trap states without physically removing them from the layer through the physisorption of molecules on the sulfur vacancy, as demonstrated for MoS_2 monolayers.[23]

In this work, we study the impact of physisorbed molecules on the electronic properties of the WSe_2 monolayer by employing state-of-the-art DFT and AIMD calculations. To this end, we explore the effects caused by molecules with diverse electron affinities, namely, C_{20}, C_{26}, C_{60}, TTF, TCNQ, TCNE, and F_4-TCNQ, which are commonly used to functionalize MoS_2 monolayers. Our molecular set also includes a strong electron-donating molecule (TTF) and strong electron acceptors (TCNQ and F_4-TCNQ). The intermediate cases are represented by considering fullerenes (C_{20}, C_{26}, and C_{60}). We show that molecular adsorption tunes the electronic properties of WSe_2 and modifies its work function. Interestingly, the V_{Se} trap states can be also affected by the presence of molecules on the surface of a defective WSe_2 monolayer.

2. COMPUTATIONAL DETAILS

The DFT calculations were performed using the projector-augmented wave basis set, as implemented in the VASP suite of codes.[40,41] We treated the exchange and correlation effects within the generalized gradient approximation (GGA) scheme, developed by Perdew−Burke−Ernzerhof (PBE),[42] and incorporated the dispersion forces using the Grimme DFT-D2 correction.[43] This quantum chemical approach typically depicts suitably interfacial effects for large systems where dispersion forces are of general importance. We also verified the equilibrium geometries by using the vdW-DF XC functional for several specific cases.[44] To obtain more reliable electronic band gaps and hence energy level alignments, we further used the hybrid functional Heyd−Scuseria−Ernzerhof (HSE06) with a range separation parameter of 0.2 $Å^{-1}$[45] in single-point self-consistent calculations. We also accounted for the spin−orbit coupling interaction for selected systems to assess its effect on the band gap and band alignment. We used an energy cutoff of 550 eV for the plane-wave basis set and a k-mesh of 3 × 3 × 1 for the Brillouin zone (BZ) integrations. A 5 × 5 × 1 supercell was constructed to simulate the WSe_2/molecular heterostructures. A dipole correction scheme was applied along the Z-direction in all calculations. During the geometry relaxation, the convergence criteria for the residual force and energy were set to 10^{-3} eV/Å and 10^{-5} eV, respectively. The time evolution of the TTF and TCNQ configurations over the WSe_2 substrate was examined by Born-Oppenheimer ab initio molecular dynamics (AIMD) simulations, as implemented in VASP by using the canonical ensemble (*NVT*) with a Nose-Hoover thermostat. The systems were equilibrated at 300 K, and a trajectory of a total simulation time of 6 ps with a time step of 1 fs was collected to analyze the dynamical properties.

The adsorption energy was calculated by the following equation

$$E_a = E_{tot} - E_{WSe2} - E_{molecule} \quad (1)$$

where E_{tot}, E_{WSe2}, and $E_{molecule}$ are the total energies of the full heterostructure, isolated WSe_2 monolayer, and isolated molecules (C_{26}, C_{60}, C_{20}, TTF, TCNQ, and F_4-TCNQ), respectively.

The chemical potential is defined as follows

$$\mu = \frac{1}{2}(E_{CBM} + E_{VBM}) \quad (2)$$

where E_{VBM} (E_{CBM}) denotes the energy of the molecular HOMO (LUMO) level for the molecules and the energy of VBM (CBM) for the WSe_2 with respect to the vacuum level. Note that this choice of energy levels is a commonly used approximation to substitute the ionization potential and electron affinity.

Due to the withdrawal/injection of electrons from/to WSe_2 by molecules, a vacuum level shifting ΔV [i.e., a difference between the electrostatic potential at the right side of the heterostructure (E_{right}) and the value at the left side (E_{left}), $\Delta V = E_{left} - E_{right}$] can be induced across the interface. ΔV induces a modification in work function

$$\Phi_{WSe2/molecule} = \Phi_{WSe2} - \Delta V \quad (3)$$

where Φ_{WSe2} is the work function of pristine WSe_2. It is worth mentioning that, when a polar molecule is adsorbed on the surface, an intrinsic dipole moment adds up with the charge transfer contribution to modify the work function. The total vacuum level shift is then given as follows

$$\Delta V = \Delta V_{BD} + \Delta V_M \quad (4)$$

where ΔV_{BD} is the contribution of charge transfer (bond dipole) and ΔV_M is the contribution of the out-plane dipole moment of the molecules.

The formation energy of an isolated V_{Se} vacancy defect is calculated by the following equation[46]

https://doi.org/10.1021/acsaelm.2c01718
ACS Appl. Electron. Mater. 2023, 5, 1660−1669

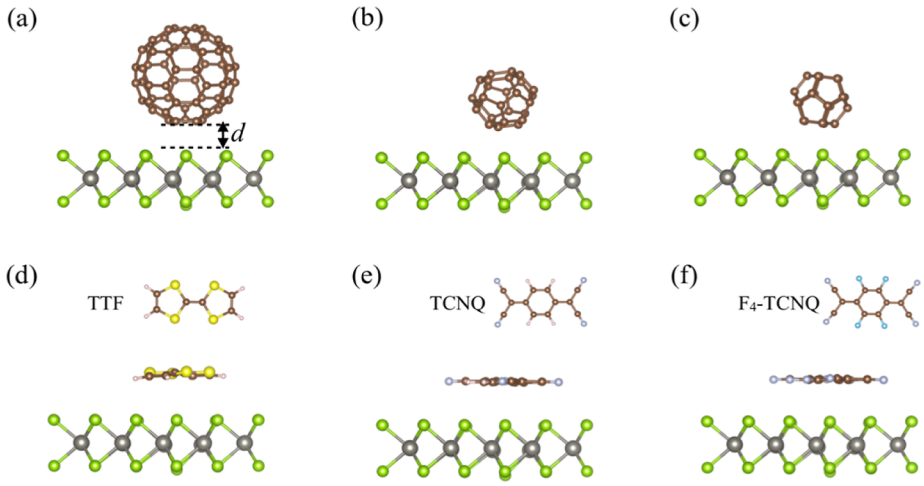

Figure 1. Most stable configurations of WSe_2/molecule heterostructures obtained after geometric relaxation: (a) WSe_2/C_{60}, (b) WSe_2/C_{26}, (c) WSe_2/C_{20}, (d) WSe_2/TTF, (e) WSe_2/TCNQ, and (f) WSe_2/F_4-TCNQ.

Table 1. Adhesion Energy E_a (eV), Interlayer Distance d (Å), Bader Charge Q on WSe_2 (|e|), Work Function W_f (eV), Vacuum Level Shift ΔV (eV), and Dipole Moment μ_{oz} (D) for the Molecular Heterostructures of WSe_2[a]

system	E_a (eV)	d (Å)	Q_{Bader} (|e|)	W_f (eV)	ΔV (eV)	μ_{oz} (D)	exp.
WSe_2/C_{20}	−0.65 (−0.76[28])	2.99 (3.02[28])	−0.02	4.41	+0.07	−0.37	
WSe_2/C_{26}	−0.80 (−0.99[28])	2.78 (2.87[28])	+0.043	4.61	−0.13	+1.14	
WSe_2/C_{60}	−1.06 (−0.84[27])	2.70 (2.91[27])	+0.01	4.59	−0.11	+0.77	p-type[51]
WSe_2/TTF	−0.93 (−0.67[22])	3.00 (3.04[22])	−0.051	4.40	+0.08	−0.49	n-type[30]
WSe_2/TCNQ	−1.26 (−0.84[22])	3.10 (3.33[22])	+0.16	4.78	−0.29	+1.97	p-type[30]
WSe_2/F_4-TCNQ	−1.50	3.06	+0.34	4.89	−0.41	+2.67	p-type

[a]The values in brackets are for MoS_2 taken from previous works.

$$E^f[V_{Se}] = E[V_{Se}^q] - E[WSe_2] + \mu_{Se} + qx(E_{VBM} + E_f) + E_{corr} \quad (5)$$

and for the substitutional carbon defect as follows

$$E^f[V_{Se}] = E[V_{Se}^q] - E[WSe_2] + \mu_{Se} - \mu_C + qx(E_{VBM} + E_f) + E_{corr} \quad (6)$$

where $E[V_{Se}{}^q]$ is the total energy of a supercell WSe_2 containing a Se vacancy in the charge state q, $E[WSe_2]$ is the total energy of a pristine supercell WSe_2, μ_{Se} is the chemical potential of the Se atom, q is the charge state of the defect, E_{VBM} is the VBM level of pristine WSe_2, E_f is the Fermi level energy of the undoped system with respect to E_{VBM}, and E_{corr} is the total energy correction, including the band level alignment and removing the spurious electrostatic interaction between image charges in supercells for charged defects, which is calculated by using the sxdefectalign2d code.[47] Under the Se-rich limit condition, the Se monoclinic crystal is chosen as a Se reservoir, and μ_{Se} is the total energy of the Se monoclinic crystal per atom. Note that the μ_C is chosen as the total energy of a C atom in different fullerene molecules and bulk diamond.

3. RESULTS AND DISCUSSION

3.1. Molecular Adsorption on the Pristine WSe_2 Monolayer. To begin with, we analyzed the structural parameters and electronic properties of an isolated WSe_2 monolayer. The calculated lattice constants at the PBE level are $a = b = 3.31$ Å. These values are in agreement with other calculations and differ from the experimental value by only 1%.[48] In the relaxed structure, the W−Se bond length is 2.54 Å and the W−Se−W bond angle is 82.42°; the thickness of the atomic layers is 3.35 Å, which is also in good agreement with other theoretical calculations.[26] For a pristine WSe_2 monolayer, we obtained a direct band gap of 2.04 eV at the HSE06 level, which is also consistent with previous theoretical results.[16,49,50] This value is higher by about 0.53 eV than the band gap value of 1.51 eV obtained at the level of GGA-PBE. For the sake of comparison, the band gap at the HSE06 level with spin−orbit coupling (SOC) is found to be 1.71 eV. This indicates that the SOC significantly decreases the band gap of the WSe_2 monolayer by about 0.34 eV; error cancellation thus ensures a reasonable estimation of the band gap by the PBE functional. The detailed characterization of orbital compositions of the VBM and CBM at the K-point is summarized in Table S1, which are calculated by projecting the orbitals onto spherical harmonics for each band. The valence band maximum (VBM) of the WSe_2 monolayer is dominated by W_{-dxy} orbitals (∼41.33%) and $W_{-dx2-y2}$ orbitals (∼41.33%), with a contribution from Se_{-px} orbitals (∼8.62%) and Se_{-py} orbitals (∼8.62%). The CBM is mainly composed of W_{-dz2} (85.38%) and W_{-s} (∼9.53%) orbitals with a small admixture of Se_{-px} (∼3%) and Se_{-py} (∼3%), which is in good agreement with other reported results.[26]

To investigate the impact of molecular adsorption on the WSe_2 surface, we placed one molecule on top of the 5 × 5 supercell of WSe_2, resulting in an adsorption areal density of 0.39 mol/nm^2 for all adsorbed molecules. Note that the shortest distance between the molecules and their periodic images was found to be ∼7 Å; therefore, the molecules can be considered nearly isolated. Due to different possible molecular

https://doi.org/10.1021/acsaelm.2c01718
ACS Appl. Electron. Mater. 2023, 5, 1660−1669

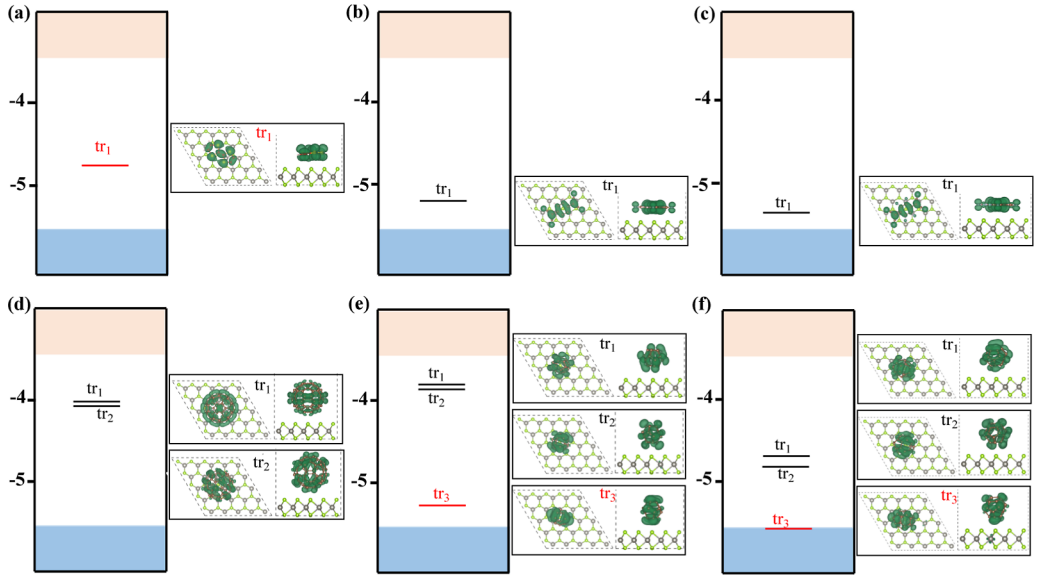

Figure 2. Energy band alignments relative to the vacuum level, the molecular levels acting as trap states within the band gap of the WSe_2 monolayer, and corresponding molecular wavefunctions for: (a) WSe_2/TTF, (b) WSe_2/TCNQ, (c) WSe_2/F_4-TCNQ, (d) WSe_2/C_{60}, (e) WSe_2/C_{20}, and (f) WSe_2/C_{26}. The red and black lines denote the occupied and unoccupied states, respectively. The orange and blue areas correspond to the conduction and valence bands of WSe_2, respectively. The energy band alignment calculated at the GGA-PBE level is depicted in Figure S2. The band alignment for F_4-TCNQ adsorption is depicted in Figure S3.

orientations, we first tested several adsorption sites (typically, five configurations of different molecular orientations relative to the plane of WSe_2) to identify the thermodynamically most stable molecular configurations on the basal surface of WSe_2. The resulting configurations are shown in Figure 1, and the corresponding adhesion energies and equilibrium distances (between the top-most atoms of the WSe_2 monolayer and the bottom-most atoms of the molecules) are summarized in Table 1. For the sake of comparison, in Tables 1 and S1, we summarized the adsorption energies, interlayer distances, and transferred charge for the molecule/MoS_2 heterostructures, taken from the literature. For each molecule, we found negative values for E_a. This implies that the molecular adsorption is thermodynamically favorable, which also suggests the experimental feasibility of the proposed functionalization.

More specifically, the fullerene molecules are preferentially adsorbed on the WSe_2 monolayer in a configuration where the nearest carbon rings are centered atop one Se atom. The equilibrium separation distances are 2.99 Å (WSe_2/C_{20}), 2.78 Å (WSe_2/C_{26}), and 2.70 Å (WSe_2/C_{60}), and the adhesion energies per molecule are −0.65, −0.80, and −1.06 eV, respectively. The equilibrium structures are similar to those of MoS_2/molecular complexes (used thereafter for the sake of reference), namely, MoS_2/C_{20},[28] MoS_2/C_{26},[28] and MoS_2/C_{60},[27] in terms of the preferential orientation around the S-atop site, as obtained at the same level of theory. The adhesion energy of WSe_2/C_{60} is larger than that of MoS_2/C_{60} or WS_2/C_{60}, and the separation distance is smaller; this points to a stronger interaction of C_{60} with WSe_2 than with WS_2 or MoS_2 monolayers. For the adsorbed TTF, the two dithiolylidene rings are eclipsing the two hollow rings of WSe_2, which is in line with the physisorbed configuration for a MoS_2/TTF heterostructure.[22] The equilibrium distance between TTF and WSe_2 is 3.01 Å, and E_a is −0.93 eV. The most stable configurations for both F_4-TCNQ and TCNQ are achieved when the centers of carbon hexagons are situated on top of a Se atom, again similar to reported results for F_4-TCNQ and TCNQ on the MoS_2 monolayer.[21,22] The adhesion energies of TCNQ and F_4-TCNQ on WSe_2 are −1.26 and −1.50 eV, respectively, which are slightly larger than that of MoS_2/TCNQ heterostructures.[22] The computed vertical distances (d) are 3.10 and 3.06 Å for TCNQ and F_4-TCNQ, respectively. In the case of TCNQ, it is slightly shorter than that for MoS_2/TCNQ (3.06 Å versus 3.33 Å, respectively).[22] Altogether, while the molecules/WSe_2 complexes show clear structural similarities with those obtained with MoS_2, we infer that WSe_2 interacts in a stronger way with both donor and acceptor molecules. To verify the accuracy of empirical Grimme's correction in the calculation of interlayer distances, we studied the adsorption of C_{20}, C_{26}, and C_{60} with the vdW-DF XC functional. We found that the interlayer distances increase by only 0.1−0.2 Å with vdW-DF as compared to results obtained by DFT-D2, which should not alter the general conclusions of this work.

To assess the modifications of the electronic properties of WSe_2 induced by the presence of a molecular dopant, we proceeded with the analysis of the electronic structures along with the shape of frontier orbitals. The energy level alignment of VBM, CBM, and induced trap states for each molecule adsorbed on the WSe_2 monolayer is shown in Figure 2 (see also Figures S1−S3 and Table S2). The effect of SOC was further mimicked by performing PBE calculations due to the similarities in the band gap and band alignment with the HSE + SOC results. Note that the PBE and HSE results provide a qualitatively consistent picture with the only difference being a rigid shift in the energy levels, see Figure S4.

The effects of the physisorbed molecules on the electronic properties of the WSe_2 monolayer can be evidenced by a comparison between the band structure of the pristine WSe_2 and those of WSe_2/molecular complexes. As shown in Figure 2, most of the physisorbed molecules introduce localized levels within the band gap of WSe_2 without significantly modifying the nature of VBM and CBM of WSe_2. Depending on the molecular nature, these trap states may either act as acceptor or

https://doi.org/10.1021/acsaelm.2c01718
ACS Appl. Electron. Mater. 2023, 5, 1660−1669

donor states and are therefore promising for doping. The C_{60} adsorption creates two empty states within the band gap, localized at 1.43 eV (here and thereafter relative to the VBM), which exclusively originate from the orbitals of the C_{60} molecule (see Table S1 for the detailed orbital decompositions). The adsorption of C_{20} creates three band states within the band gap, with one fully occupied and localized at 0.25 eV and two empty levels localized at 1.64 and 1.72 eV. Note that all new levels are localized on C_{20}. In turn, TTF adsorption introduces a deep occupied level localized at 1.04 eV, while the TCNQ (F_4-TCNQ) gives rise to a deep empty state at 0.37 eV (0.21 eV).

Furthermore, to provide a robust description of the molecular doping of WSe_2, we plot in Figure S5 the energy level diagrams for the individual components of the heterostructures. Noteworthily, the magnitude and the flow direction of charge transfer across the interface are predominantly rationalized in terms of the difference in the chemical potentials of the constituting components. In this simplified framework, the electrons are transferred from the material with the smaller chemical potential to the material with the larger one (although the softness also plays a non-negligible role[52]). The chemical potentials for the isolated components, calculated by eq 3, are shown in Figure S5. The values for C_{60} (−5.13 eV), C_{26} (−5.1 eV), C_{20} (−4.50 eV), TCNQ (−6.36 eV), and F_4-TCNQ (−6.78 eV) are larger than that of pristine WSe_2 (−4.48 eV). This induces an electron transfer from the WSe_2 monolayer to the molecules and results in a p-type doping of WSe_2. Surprisingly, the interfacial interaction of C_{60} with MoS_2 and WS_2 has been shown to result in n-doping.[27] Our result for C_{60} agrees with the spectroscopic observation of C_{60}, causing p-doping in WSe_2.[51] The Bader charge analysis yields a charge transfer, from WSe_2 to the molecule, of +0.02 |e|, +0.01 |e|, +0.043 |e|, +0.16 |e|, and +0.34 |e| (where "e" is the elementary electron charge) for C_{20}, C_{60}, C_{26}, TCNQ, and F_4-TCNQ, respectively. In turn, this gives rise to a dipole moment oriented toward the molecules, see the calculated values in Table 1. On the other hand, an opposite scenario is observed for the TTF/WSe_2 monolayer, where the smaller chemical potential of TTF (−3.01 eV) compared to WSe_2 (−4.48 eV) induces an n-type doping, as confirmed by a charge transfer of −0.051 |e|. As expected from the large electron-withdrawing effect of cyano groups and fluorine atoms, the largest difference in chemical potential between WSe_2 and F_4-TCNQ yields the largest amount of charge transferred. Note that the induced dipole moment at the interface is one important factor to separate photogenerated electron−hole pairs.[53−55] Under light exposure, it can promote the splitting of the photoexcited excitons, driving the charge carriers to the different sides of the heterostructure. Hence, this effect is very helpful to improve the efficiency of the WSe_2 monolayer in photocatalytic and photovoltaic applications.

Next, we studied the modifications in the work function of WSe_2 due to the creation of an electrical dipole moment at the WSe_2/molecular interfaces. This effect can be captured by computing the plane-averaged electrostatic potential across the full system and assessing the difference between the vacuum level energies at the right and left sides of the slab [$\Delta V = E_{left} - E_{right}$], as shown in Figure S6. For the pristine WSe_2, the electrostatic potential is symmetric with respect to the basal plane and the computed work function is 4.48 eV. This value reflects the effective position of the Fermi level in the pristine materials relative to the vacuum level and is in a good agreement with other theoretical studies.[26,56] Molecular adsorption leads to a characteristic vacuum level shift (ΔV), as summarized in Table 1. More specifically, due to a weak charge transfer, the work function of WSe_2 changes upon adsorption of C_{20}, C_{26}, and C_{60}, reaching the values of 4.41, 4.61, and 4.59 eV, respectively. The strong charge transfer upon TCNQ and F_4-TCNQ adsorption directly translates into a significant increase in the work function up to 4.78 and 4.86 eV, respectively. In contrast, due to the n-type doping induced by TTF, a decrease of the work function down to 4.40 eV is observed.

3.2. Effect of Coverage Density on Physisorption.

Next, having described the effects induced by isolated molecules, we investigated the impact of coverage density on the strength of doping. Here, an increased density of organic dopants can lead to the formation of new molecular configurations, caused by the mutual interaction between molecules; this can either yield variations in the interface distances or molecular reorientations. To mimic these effects in our calculations, we increased the molecular density by reducing the size of the supercell, focusing on two representative molecules, namely, an electron donor (TTF) and electron acceptor (TCNQ). Note that these models are essentially useful to capture an effect of the enhanced $\pi-\pi$ interactions within the organic layer. The resulting high coverage density was 0.76 mol/nm^2. The equilibrium structures of the interfaces after geometry relaxation are depicted in Figure S7. The increase in coverage density leads to a considerable modification in the structural parameters of the heterostructures, as evidenced by an inclination of the molecules relative to the basal-plane surface of WSe_2 by 17°. More specifically, the interlayer distance, computed as the difference between the top-most atoms of WSe_2 and the center of the molecules, increases by ∼8% for TTF and 3.4% for TCNQ, which indicates that the molecules tend to move further apart from the WSe_2 surface. This destabilization of the heterostructure is also seen from a decrease in adhesion energies by ∼13% (see Table S3), which is compensated by enhanced $\pi-\pi$ interaction between the molecules.[57] The Bader charge analysis shows a decrease in the charge transfer per molecule at the higher density (from 0.051 to 0.03 |e| for TTF adsorption and from 0.16 to 0.13 |e| for TCNQ), which is associated with the so-called electronic depolarization effects[58] and the increase in the interlayer distances. Clearly, TCNQ is found to be more robust against depolarization, owing to its rigid structure. As a result, the total amount of charge transfer per surface area is significantly increased, leading in turn to an increase in the work function of the WSe_2 monolayer. Experimental measurements[19] also revealed the same tendency when increasing the concentration of small solvent molecules adsorbed on both MoS_2 and WSe_2 monolayers.

Moreover, from the experimental point of view, this effect is even more pronounced than in our static DFT calculations. For instance, it has been reported that when an effective dopant such as F_4-TCNQ is densely packed on an epitaxial graphene film, most of the molecules are standing up.[59] To elaborate on the difference with experiment, we performed additional AIMD calculations in the canonical ensemble (NVT), at an average temperature of 300 K controlled by employing a Nosé-Hoover thermostat. The energy profile during a trajectory of 6 ps is shown in Figure S8. The basal structure geometry of the WSe_2 monolayer remains intact

https://doi.org/10.1021/acsaelm.2c01718
ACS Appl. Electron. Mater. 2023, 5, 1660−1669

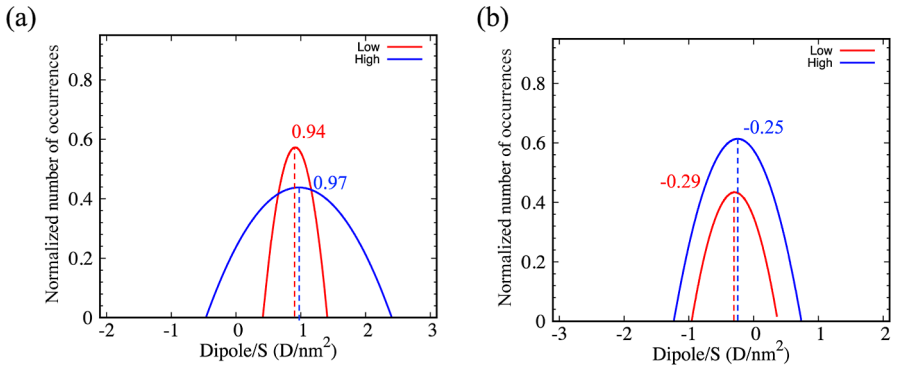

Figure 3. Evolution of the total dipole during the trajectory of 6 ps from AIMD calculations: (a) WSe_2/TCNQ and (b) WSe_2/TTF, with low-density coverage (red curves) and high-density coverage (blue curves).

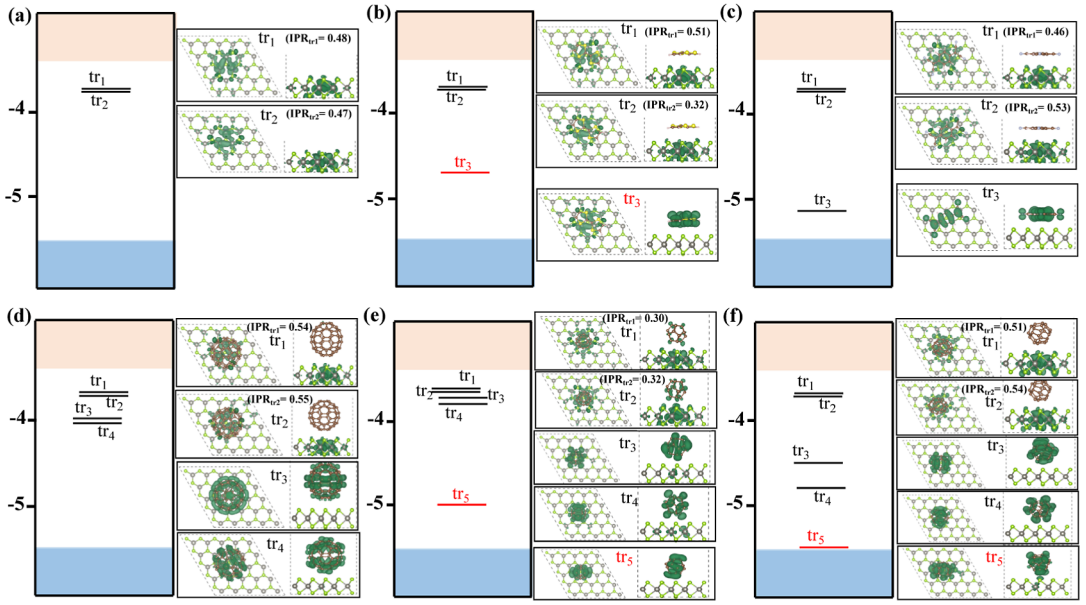

Figure 4. Trap states within the band gap of defective WSe_2 and their corresponding wavefunctions: (a) with a Se vacancy and (b) TTF, (c) TCNQ, (d) C_{60}, (e) C_{20}, and (f) C_{26} adsorption. The red and black lines denote the occupied and unoccupied states, respectively. The orange and blue areas correspond to the conduction and valence bands of WSe_2, respectively.

within 6 ps; however, different configurations are observed for the physisorbed molecules. Noteworthily, the (otherwise flat) molecules become buckled; this breaks the molecular symmetry and induces an additional non-negligible surface dipole moment, as seen from the significant fluctuations of the total dipole moment during the 6 ps of the dynamics, see Figure S9 in the Supporting Information. The distribution of the total dipole moments during the simulation is presented in Figure 3. A broad distribution of the total dipole moments is found in both cases. Moreover, the average value of the dipole moment slightly shifts from the low coverage density to the high coverage regime. Noteworthily, the direction of the shift reflects the change in the total amount of transferred charge per surface area for a given dopant. Thus, the total dipole of TCNQ slightly increases toward the high coverage, while it decreases for TTF. For the latter, we also tested a higher density of 1.36 mol/nm^2 and found an even larger decrease along the same direction, see Figure S10.

For the sake of completeness, we also examined the charge transfer and resulting work function changes for two noteworthy configurations, which were extracted from the molecular dynamics trajectory, as depicted in Figure S11. As evidenced by the values in Table S3, the buckling of the molecule structure leads to only a slight change in the amount of charge transfer; however, it yields a significant modification in the work function. This result can be understood from the out-of-plane component of the molecular dipole moment of the buckled molecule that adds up to the charge transfer contribution to the work function change. Such effects associated to an intrinsic molecular dipole were also observed, both experimentally and theoretically, with polar molecules physisorbed on the MoS_2 monolayer.[20]

3.3. Molecules Adsorbed above a Se Vacancy of the WSe_2 Monolayer. In this section, we examine the structural and electronic properties of adsorbed molecules on a WSe_2 monolayer containing a single Se vacancy (V_{Se}) in the top layer. Given the size of the 5 × 5 supercell of the WSe_2 monolayer, we considered a single neutral selenide vacancy defect, i.e., with a density of 2%. The recalculated interlayer distances and adhesion energies are summarized in Table S4. The noteworthy effects of the Se vacancy on the hetero-structure are an increase in the adhesion energy (by ∼8.5%) and a decrease in the interlayer distance (by ∼5.1%). This points to an enhancement of the interaction strength between

https://doi.org/10.1021/acsaelm.2c01718
ACS Appl. Electron. Mater. 2023, 5, 1660−1669

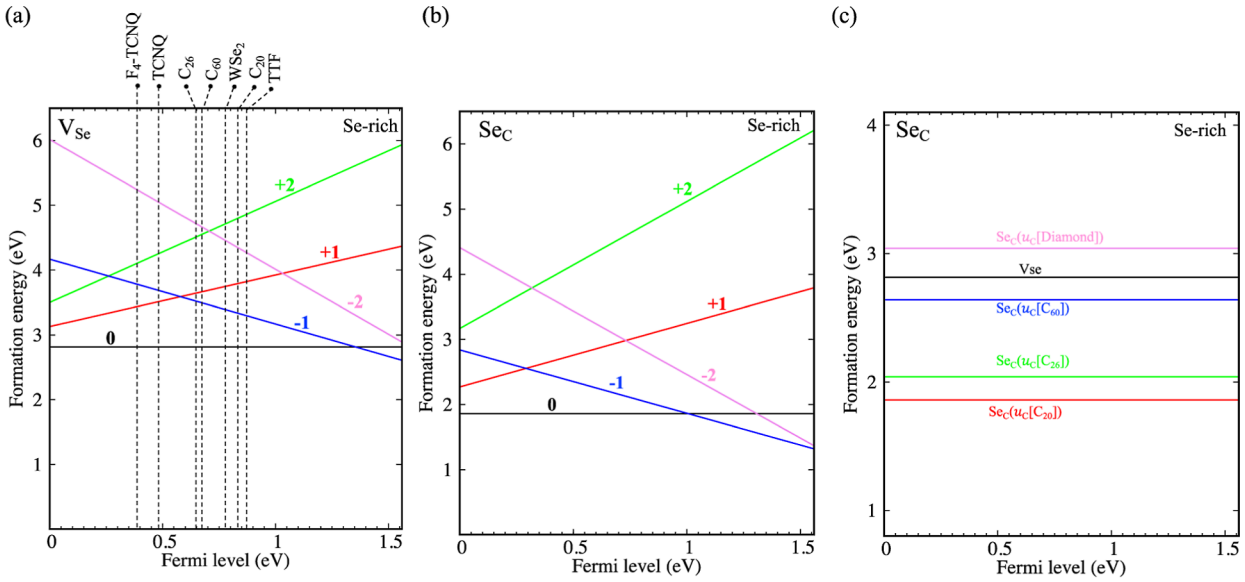

Figure 5. Calculated formation energies of (a) an isolated V_{Se} in a WSe_2 monolayer and (b) substitutional carbon defect in the WSe_2 monolayer in various charge states as a function of the Fermi level using the Se-rich condition. (c) Calculated formation energies of a neutral substitutional carbon defect in the WSe_2 monolayer using different reference values of μ_C.

the defected WSe_2 monolayer and the physisorbed molecules due to the presence of V_{Se}.

The HSE-calculated energy band alignments of defective WSe_2 versus adsorbed molecules are shown in Figure 4 (those calculated at the GGA-PBE level are depicted in Figure S12). The band structure of WSe_{v2}, Figure 4a, shows the appearance of two nearly degenerate unoccupied states (tr_1 and tr_2) within the band gap localized 0.32 eV below CBM; this observation is in line with other theoretical calculations.[31] These two trap states (tr_1 and tr_2) are splitted by an energy of 0.02 eV. Note that the energy splitting is calculated to be 0.18 upon including the spin−orbit coupling, as shown in Figure S13 and Table S5. Analysis of the orbital characters (see Table S6) demonstrates that the induced trap states originate from a hybridization between W_{-d} orbitals [$W_{-dx2-y2}$ (33.33%), W_{-dxz} (7.52%), % W_{-dz2} (13.41), W_{-dxy} (13.40%), and W_{-dyz} (13.41%)] and Se_{-p} orbitals [Se_{-px} (5.77%), Se_{-py} (8.65%), and Se_{-pz} (3.89%)]. As evidenced by the shape of the crystalline orbitals in Figure 4a, these trap states are mostly localized on the W atoms surrounding the vacancy site.

The Se vacancy leads to a slight increase (by ∼5%) in the work function (up to 4.56 eV) as compared to the pristine layer, indicating p-type doping. Upon molecular adsorption, the trap states associated with Se vacancy are renormalized. Interestingly, in contrast to a defect in the pristine material, molecular adsorption causes a shift in the position of the defect levels, suggesting a change in the charge density. This is induced by an apparent hybridization with the molecular levels, as shown in Figure 4. Moreover, the shifting in the gap states is also due to a change in the amount of the charge transfer and hence in the induced dipole moment at the interface. The Bader charge analysis points to a decrease (by about 5%) in the charge transfer between the defective WSe_2 monolayer and acceptor molecules, while a huge increase (by 50%) is calculated in the case of TTF donor molecules.

Now, we assess the effect of the physisorption of molecules on the charge states of V_{Se}. To this end, we closely followed the methodology of ref 46 to calculate the formation energy of V_{Se} in the (+2), (+1), (0), (−1), and (−2) charge states. The calculated formation energies as a function of Fermi level (under the Se-rich condition) are plotted in Figure 5a. The most stable charge states of V_{Se} are found to be (0) and (−1), given the Fermi level inside the band gap. The calculated absolute values of formation energy range between 2.81 and 2.61 eV depending on the position of the Fermi level. The (0/−1) transition level is found at $\varepsilon(0/-1) = E_{VBM} + 1.36$ eV; this means that V_{Se} can act as a deep acceptor in the WSe_2 monolayer and can trap an electron in a typical n-type WSe_2, forming V_{Se}^{1-}. Note that our results for WSe_2 are qualitatively similar to the reported formation energy diagram for V_S in the MoS_2 monolayer.[46]

Furthermore, an experimental study suggests that the chalcogenide vacancies in TMDs are reactive and can remove carbon atoms from adsorbed carbon-based molecules.[60] To elaborate on this, we calculated the formation energies of a substitutional C-defect in WSe_2 in the (+2), (+1), (0), (−1), and (−2) charge states. We considered C_{20}, C_{26}, and C_{60} as the source of carbon, providing different values of μ_C, and also used bulk diamond as the reference. The formation energy of C-defect in different charge states is shown in Figure 5b. Interestingly, we found that the (−1) and (−2) charge states of C-defect are stabilized by 0.3 eV relative to V_{Se}, as evidenced by a shift of the (0/−1) charge transition level from E_{VBM} + 1.36 eV to E_{VBM} + 1.06 eV. This indicates that the adsorption of carbon enhances the acceptor function of the native defect in WSe_2. Considering now the different sources of the C atom, we found that the relative stability of C-defect and V_{Se} depends on μ_C. In particular, large molecular strain in small fullerenes leads to an easier formation of C-defect, as observed from the formation energies in Figure 5c. The direct DFT calculations for C_{26} and V_{Se} confirm the thermodynamically favorable removal of carbon from the molecule, which is stabilized by a formation of the C−C bond between the C_{25} and C-defect units. Remarkably, this configuration shows the transferred charge of 0.81 |e| from WSe_2, which is the largest value for the systems under consideration.

Another possible relevant effect of molecular adsorption on the defective WSe_2 is an ability to manipulate the position of

https://doi.org/10.1021/acsaelm.2c01718
ACS Appl. Electron. Mater. 2023, 5, 1660−1669

the Fermi level and hence to stabilize the defect charge states of interest. To elaborate on this point, we first fixed the Fermi level in the middle of the band gap of pristine WSe_2 and then compared the variations in the formation energy of heterostructures by considering the computed VLSs. The dashed lines in Figure 5a show the position of the Fermi level of heterostructures with respect to isolated WSe_2. From Figure 5a, we observe the following trends upon molecular adsorption: (i) the adsorption of C_{26} and TTF leads to further stabilization of the (−1) charge state with respect to isolated WSe_2, (ii) C_{60} and C_{26} molecules tend to destabilize both (+1) and (−1), and (iii) the large electron-withdrawing effect of strong acceptor molecules such as F_4-TCNQ and TCNQ translates into a further stabilization of the (+1) charge state. In each case, we observe that the neutral charge state is robust to molecular adsorption. Nonetheless, we anticipate that the large variations of VLS can be utilized to fine-tune the defect charge state in heterostructures and doped samples of WSe_2.

To further analyze the influence of a Se vacancy, we calculated the inverse participation ratio (IPR) for the V_{Se} trap states. Note that the IPR captures the degree of local localization so that the higher the magnitude of IPR is, the more the state is localized. The values of IPR for V_{Se} trap states are shown in Figure 4. The calculated IPR value for the trap states (tr_1 and tr_2) of WSe_2 with a V_{Se} is 0.48, which corresponds to localized states. For the sake of comparison, the IPR for the VBM and CBM of WSe_2 with a V_{Se} is found to be about ∼0.032, which implies a larger degree of local orbital delocalization at the band edges. A significant modulation in the IPR values is observed upon molecular adsorption. The effect is particularly pronounced for C_{20}, where the values of IPR are reduced by 35% (for both trap states tr_1 and tr_2); this implies that the molecular levels of C_{20} contribute to a delocalization of the trap states. In turn, TTF gives rise to an asymmetric modification of the levels; the IPR is reduced by about 33% (from 0.48 to 0.32) for tr_2, while only a small change is found for tr_1. By contrast, the adsorption of TCNQ, F_4-TCNQ, C_{60}, and C_{26} molecules induces only a minor modification in the degree of localization of V_{Se} trap states.

4. CONCLUSIONS

In summary, we have investigated the impact of molecular physisorption on the electronic structure and work function of pristine and defective WSe_2 monolayers. The most used molecules for functionalizing TMDs have been selected, namely, fullerenes (C_{20}, C_{26}, and C_{60}), TTF, TCNQ, and F_4-TCNQ molecules. These molecules are physisorbed on the WSe_2 monolayer via weak van der Waals interactions, as evidenced from the interlayer distances (ranging from 2.7 to 3.01 Å) and binding energies (from −0.65 to −1.5 eV). We show that the electronic properties and work function of the WSe_2 monolayer can be modulated and controlled by selecting a proper dopant. The charge transfer from (toward) the WSe_2 monolayer leads to an induced dipole molecule which in turn changes the work function of the material. At high coverage, the buckling and reorientation of molecules lead to out-of-plane dipole moments which further contribute to the variation of the work function of the WSe_2 monolayer. Our results also point to an enhanced interaction of the monolayer with the dopants in the presence of a single Se vacancy. Interestingly, the localized defect levels can also hybridize with those of the molecules, which leads to a modification of the defect properties in terms of energy levels and degrees of delocalization. Moreover, the calculated formation energies of charged states of V_{Se} in a WSe_2 monolayer have shown a significant effect of adsorbed molecules on the stability of charged defect states upon variation of the Fermi level position. We have also demonstrated that fullerenes can chemically bound to WSe_2 owing to the presence of reactive vacancies in the material. As shown for C_{26}, this process can greatly enhance an electron withdrawal effect of the molecule. The present results could pave the way toward a potential engineering of defect properties in 2D TMDs for efficient applications in optoelectronic devices.

■ ASSOCIATED CONTENT

Supporting Information

The Supporting Information is available free of charge at https://pubs.acs.org/doi/10.1021/acsaelm.2c01718.

Orbital characters of the VBM and CBM for the pristine WSe_2 and heterostructures; band structures of a WSe_2 monolayer and heterostructures; energy band alignments at different levels of theory; averaged electrostatic potential profiles and charge transfer properties; AIMD trajectories and corresponding variations of total dipole moment; configurations of TTF/WSe_2 and TCNQ/WSe_2, extracted from the molecular dynamics trajectories; and energy diagrams for the defected heterostructures, showing the defect states and molecular levels within the band gap of WSe_2 (PDF)

■ AUTHOR INFORMATION

Corresponding Authors

Amine Slassi − *Istituto Nanoscienze-CNR, Modena I-41125, Italy;* orcid.org/0000-0001-5877-6045; Email: amine.slassi@nano.cnr.it

Adam Gali − *Wigner Research Centre for Physics, Budapest H-1525, Hungary; Department of Atomic Physics, Budapest University of Technology and Economics, Budapest H-1111, Hungary;* orcid.org/0000-0002-3339-5470; Email: gali.adam@wigner.hu

Anton Pershin − *Wigner Research Centre for Physics, Budapest H-1525, Hungary; Department of Atomic Physics, Budapest University of Technology and Economics, Budapest H-1111, Hungary;* orcid.org/0000-0002-2414-6405; Email: pershin.anton@wigner.hu

Author

Jérôme Cornil − *Laboratory for Chemistry of Novel Materials, University of Mons, Mons 7000, Belgium;* orcid.org/0000-0002-5479-4227

Complete contact information is available at: https://pubs.acs.org/10.1021/acsaelm.2c01718

Notes

The authors declare no competing financial interest.

■ ACKNOWLEDGMENTS

This work was supported by the Belgian National Fund for Scientific Research (FRS-FNRS), Wallonie-Bruxelles International (WBI), and Region of Wallonie (RW) within the project of 2D Materials and FNRS-TOREADOR project. Computational resources were provided by the Consortium des Équipements de Calcul Intensif (CÉCI) funded by F.R.S.-FNRS under grant 2.5020.11. A.M. acknowledges the financial

support from EC through the H2020-DT-NMBP-11-2020 project GA no. 953167 (OpenModel). A.G. acknowledges the financial support from the National Research, Development and Innovation Office in Hungary (NKFIH) grant no. KKP129866 (National Excellence Program) as well as from the Quantum Information National Laboratory sponsored via the Ministry of Innovation and Technology of Hungary. J.C. is an FNRS research director. We also thank Dr. Arrigo Calzolari (CNR Researcher) for his fruitful comments.

REFERENCES

(1) Er, D.; Ye, H.; Frey, N. C.; Kumar, H.; Lou, J.; Shenoy, V. B. Prediction of Enhanced Catalytic Activity for Hydrogen Evolution Reaction in Janus Transition Metal Dichalcogenides. *Nano Lett.* **2018**, *18*, 3943−3949.
(2) Karmodak, N.; Bursi, L.; Andreussi, O. Oxygen Evolution and Reduction on Two-Dimensional Transition Metal Dichalcogenides. *J. Phys. Chem. Lett.* **2022**, *13*, 58−65.
(3) Chhowalla, M.; Shin, H. S.; Eda, G.; Li, L.-J.; Loh, K. P.; Zhang, H. The Chemistry of Two-Dimensional Layered Transition Metal Dichalcogenide Nanosheets. *Nat. Chem.* **2013**, *5*, 263−275.
(4) Koppens, F. H. L.; Mueller, T.; Avouris, P.; Ferrari, A. C.; Vitiello, M. S.; Polini, M. Photodetectors Based on Graphene, Other Two-Dimensional Materials and Hybrid Systems. *Nat. Nanotechnol.* **2014**, *9*, 780−793.
(5) Akinwande, D.; Petrone, N.; Hone, J. Two-Dimensional Flexible Nanoelectronics. *Nat. Commun.* **2014**, *5*, 5678.
(6) Radisavljevic, B.; Radenovic, A.; Brivio, J.; Giacometti, V.; Kis, A. Single-Layer MoS2 Transistors. *Nat. Nanotechnol.* **2011**, *6*, 147−150.
(7) Mak, K. F.; Lee, C.; Hone, J.; Shan, J.; Heinz, T. F. Atomically Thin MoS2: A New Direct-Gap Semiconductor. *Phys. Rev. Lett.* **2010**, *105*, 136805.
(8) Bertolazzi, S.; Brivio, J.; Kis, A. Stretching and Breaking of Ultrathin MoS 2. *ACS Nano* **2011**, *5*, 9703−9709.
(9) Britnell, L.; Ribeiro, R. M.; Eckmann, A.; Jalil, R.; Belle, B. D.; Mishchenko, A.; Kim, Y. J.; Gorbachev, R. V.; Georgiou, T.; Morozov, S. V.; Grigorenko, A. N.; Geim, A. K.; Casiraghi, C.; Neto, A. H.; Novoselov, K. S. Strong Light-Matter Interactions in Heterostructures of Atomically Thin Films. *Science* **2013**, *340*, 1311−1314.
(10) Barré, E.; Incorvia, J. A. C.; Kim, S. H.; McClellan, C. J.; Pop, E.; Wong, H.-S. P.; Heinz, T. F. Spatial Separation of Carrier Spin by the Valley Hall Effect in Monolayer WSe 2 Transistors. *Nano Lett.* **2019**, *19*, 770−774.
(11) Stoeckel, M.-A.; Gobbi, M.; Leydecker, T.; Wang, Y.; Eredia, M.; Bonacchi, S.; Verucchi, R.; Timpel, M.; Nardi, M. V.; Orgiu, E.; Samorì, P. Boosting and Balancing Electron and Hole Mobility in Single- and Bilayer WSe_2 Devices via Tailored Molecular Functionalization. *ACS Nano* **2019**, *13*, 11613−11622.
(12) Li, D.; Wang, X.; Chen, Y.; Zhu, S.; Gong, F.; Wu, G.; Meng, C.; Liu, L.; Wang, L.; Lin, T.; Sun, S.; Shen, H.; Wang, X.; Hu, W.; Wang, J.; Sun, J.; Meng, X.; Chu, J. The Ambipolar Evolution of a High-Performance WSe_2 Transistor Assisted by a Ferroelectric Polymer. *Nanotechnology* **2018**, *29*, 105202.
(13) Zhou, H.; Wang, C.; Shaw, J. C.; Cheng, R.; Chen, Y.; Huang, X.; Liu, Y.; Weiss, N. O.; Lin, Z.; Huang, Y.; Duan, X. Large Area Growth and Electrical Properties of P-Type WSe 2 Atomic Layers. *Nano Lett.* **2015**, *15*, 709−713.
(14) Podzorov, V.; Gershenson, M. E.; Kloc, C.; Zeis, R.; Bucher, E. High-Mobility Field-Effect Transistors Based on Transition Metal Dichalcogenides. *Appl. Phys. Lett.* **2004**, *84*, 3301−3303.
(15) Chen, C.-H.; Wu, C.-L.; Pu, J.; Chiu, M.-H.; Kumar, P.; Takenobu, T.; Li, L.-J. Hole Mobility Enhancement and p -Doping in Monolayer WSe 2 by Gold Decoration. *2D Mater.* **2014**, *1*, 034001.
(16) Li, Z.; Wang, T.; Jin, C.; Lu, Z.; Lian, Z.; Meng, Y.; Blei, M.; Gao, S.; Taniguchi, T.; Watanabe, K.; Ren, T.; Tongay, S.; Yang, L.; Smirnov, D.; Cao, T.; Shi, S. Emerging Photoluminescence from the Dark-Exciton Phonon Replica in Monolayer WSe2. *Nat. Commun.* **2019**, *10*, 2469.
(17) Chen, W.; Qi, D.; Gao, X.; Wee, A. T. S. Surface Transfer Doping of Semiconductors. *Prog. Surf. Sci.* **2009**, *84*, 279−321.
(18) Presolski, S.; Wang, L.; Loo, A. H.; Ambrosi, A.; Lazar, P.; Ranc, V.; Otyepka, M.; Zboril, R.; Tomanec, O.; Ugolotti, J.; Sofer, Z.; Pumera, M. Functional Nanosheet Synthons by Covalent Modification of Transition-Metal Dichalcogenides. *Chem. Mater.* **2017**, *29*, 2066−2073.
(19) Wang, Y.; Slassi, A.; Stoeckel, M.-A.; Bertolazzi, S.; Cornil, J.; Beljonne, D.; Samorì, P. Doping of Monolayer Transition-Metal Dichalcogenides via Physisorption of Aromatic Solvent Molecules. *J. Phys. Chem. Lett.* **2019**, *10*, 540−547.
(20) Wang, Y.; Slassi, A.; Cornil, J.; Beljonne, D.; Samorì, P. Tuning the Optical and Electrical Properties of Few-Layer Black Phosphorus via Physisorption of Small Solvent Molecules. *Small* **2019**, *15*, 1903432.
(21) Wang, J.; Ji, Z.; Yang, G.; Chuai, X.; Liu, F.; Zhou, Z.; Lu, C.; Wei, W.; Shi, X.; Niu, J.; Wang, L.; Wang, H.; Chen, J.; Lu, N.; Jiang, C.; Li, L.; Liu, M. Charge Transfer within the F_4TCNQ-MoS_2 van Der Waals Interface: Toward Electrical Properties Tuning and Gas Sensing Application. *Adv. Funct. Mater.* **2018**, *28*, 1806244.
(22) Jing, Y.; Tan, X.; Zhou, Z.; Shen, P. Tuning Electronic and Optical Properties of MoS 2 Monolayer via Molecular Charge Transfer. *J. Mater. Chem. A* **2014**, *2*, 16892−16897.
(23) Cai, Y.; Zhou, H.; Zhang, G.; Zhang, Y.-W. Modulating Carrier Density and Transport Properties of MoS 2 by Organic Molecular Doping and Defect Engineering. *Chem. Mater.* **2016**, *28*, 8611−8621.
(24) Slassi, A.; Cornil, D.; Cornil, J. Theoretical Characterization of the Electronic Properties of Heterogeneous Vertical Stacks of 2D Metal Dichalcogenides Containing One Doped Layer. *Phys. Chem. Chem. Phys.* **2020**, *22*, 14088−14098.
(25) Wang, Y.; Gali, S. M.; Slassi, A.; Beljonne, D.; Samorì, P. Collective Dipole-Dominated Doping of Monolayer MoS 2 : Orientation and Magnitude Control via the Supramolecular Approach. *Adv. Funct. Mater.* **2020**, *30*, 2002846.
(26) Slassi, A.; Cornil, J. Theoretical Characterization of Strain and Interfacial Electronic Effects in Donor-Acceptor Bilayers of 2D Transition Metal Dichalcogenides. *2D Mater.* **2018**, *6*, 015025.
(27) Gan, L.-Y.; Zhang, Q.; Cheng, Y.; Schwingenschlögl, U. Photovoltaic Heterojunctions of Fullerenes with MoS 2 and WS 2 Monolayers. *J. Phys. Chem. Lett.* **2014**, *5*, 1445−1449.
(28) Luo, C.-Y.; Huang, W.-Q.; Xu, L.; Yang, Y.-C.; Li, X.; Hu, W.; Peng, P.; Huang, G.-F. Electronic Properties and Photoactivity of Monolayer MoS 2 /Fullerene van Der Waals Heterostructures. *RSC Adv.* **2016**, *6*, 43228−43236.
(29) Santos, E. J. G.; Scullion, D.; Chu, X. S.; Li, D. O.; Guisinger, N. P.; Wang, Q. H. Rotational Superstructure in van Der Waals Heterostructure of Self-Assembled C 60 Monolayer on the WSe 2 Surface. *Nanoscale* **2017**, *9*, 13245−13256.
(30) Liu, H.; Cui, M.; Dang, C.; Wen, W.; Wang, X.; Xie, L. Two-Dimensional WSe 2 /Organic Acceptor Hybrid Nonvolatile Memory Devices Based on Interface Charge Trapping. *ACS Appl. Mater. Interfaces* **2019**, *11*, 34424−34429.
(31) Zhao, Y.; Gali, S. M.; Wang, C.; Pershin, A.; Slassi, A.; Beljonne, D.; Samorì, P. Molecular Functionalization of Chemically Active Defects in WSe 2 for Enhanced Opto-Electronics. *Adv. Funct. Mater.* **2020**, *30*, 2005045.
(32) Bertolazzi, S.; Bonacchi, S.; Nan, G.; Pershin, A.; Beljonne, D.; Samorì, P. Engineering Chemically Active Defects in Monolayer MoS 2 Transistors via Ion-Beam Irradiation and Their Healing via Vapor Deposition of Alkanethiols. *Adv. Mater.* **2017**, *29*, 1606760.
(33) Lu, J.; Carvalho, A.; Chan, X. K.; Liu, H.; Liu, B.; Tok, E. S.; Loh, K. P.; Castro Neto, A. H.; Sow, C. H. Atomic Healing of Defects in Transition Metal Dichalcogenides. *Nano Lett.* **2015**, *15*, 3524−3532.
(34) Li, L.; Long, R.; Prezhdo, O. V. Why Chemical Vapor Deposition Grown MoS 2 Samples Outperform Physical Vapor Deposition Samples: Time-Domain Ab Initio Analysis. *Nano Lett.* **2018**, *18*, 4008−4014.

https://doi.org/10.1021/acsaelm.2c01718
ACS Appl. Electron. Mater. 2023, 5, 1660−1669

(35) Wang, Y.; Deng, L.; Wei, Q.; Wan, Y.; Liu, Z.; Lu, X.; Li, Y.; Bi, L.; Zhang, L.; Lu, H.; Chen, H.; Zhou, P.; Zhang, L.; Cheng, Y.; Zhao, X.; Ye, Y.; Huang, W.; Pennycook, S. J.; Loh, K. P.; Peng, B. Spin-Valley Locking Effect in Defect States of Monolayer MoS2. *Nano Lett.* **2020**, *20*, 2129.
(36) Zhou, W.; Zou, X.; Najmaei, S.; Liu, Z.; Shi, Y.; Kong, J.; Lou, J.; Ajayan, P. M.; Yakobson, B. I.; Idrobo, J.-C. Intrinsic Structural Defects in Monolayer Molybdenum Disulfide. *Nano Lett.* **2013**, *13*, 2615−2622.
(37) Komsa, H.-P.; Kotakoski, J.; Kurasch, S.; Lehtinen, O.; Kaiser, U.; Krasheninnikov, A. V. Two-Dimensional Transition Metal Dichalcogenides under Electron Irradiation: Defect Production and Doping. *Phys. Rev. Lett.* **2012**, *109*, 035503.
(38) Zhu, W.; Low, T.; Lee, Y.-H.; Wang, H.; Farmer, D. B.; Kong, J.; Xia, F.; Avouris, P. Electronic Transport and Device Prospects of Monolayer Molybdenum Disulphide Grown by Chemical Vapour Deposition. *Nat. Commun.* **2014**, *5*, 3087.
(39) Pető, J.; Ollár, T.; Vancsó, P.; Popov, Z. I.; Magda, G. Z.; Dobrik, G.; Hwang, C.; Sorokin, P. B.; Tapasztó, L. Spontaneous Doping of the Basal Plane of MoS2 Single Layers through Oxygen Substitution under Ambient Conditions. *Nat. Chem.* **2018**, *10*, 1246−1251.
(40) Kresse, G.; Marsman, M. *VASP the GUIDE*, 2012.
(41) Kresse, G.; Joubert, D. From Ultrasoft Pseudopotentials to the Projector Augmented-Wave Method. *Phys. Rev. B: Condens. Matter Mater. Phys.* **1999**, *59*, 1758−1775.
(42) Perdew, J. P.; Burke, K.; Ernzerhof, M. Generalized Gradient Approximation Made Simple. *Phys. Rev. Lett.* **1996**, *77*, 3865−3868.
(43) Grimme, S. Semiempirical GGA-Type Density Functional Constructed with a Long-Range Dispersion Correction. *J. Comput. Chem.* **2006**, *27*, 1787−1799.
(44) Dion, M.; Rydberg, H.; Schröder, E.; Langreth, D. C.; Lundqvist, B. I. Density Functional for General Geometries. *Phys. Rev. Lett.* **2004**, *92*, 246401.
(45) Heyd, J.; Scuseria, G. E.; Ernzerhof, M. Hybrid Functionals Based on a Screened Coulomb Potential. *J. Chem. Phys.* **2003**, *118*, 8207−8215.
(46) Noh, J.-Y.; Kim, H.; Kim, Y.-S. Stability and Electronic Structures of Native Defects in Single-Layer ${\mathrm{MoS}}_{2}$. *Phys. Rev. B: Condens. Matter Mater. Phys.* **2014**, *89*, 205417.
(47) Freysoldt, C.; Neugebauer, J. First-Principles Calculations for Charged Defects at Surfaces, Interfaces, and Two-Dimensional Materials in the Presence of Electric Fields. *Phys. Rev. B* **2018**, *97*, 205425.
(48) Schutte, W. J.; De Boer, J. L.; Jellinek, F. Crystal Structures of Tungsten Disulfide and Diselenide. *J. Solid State Chem.* **1987**, *70*, 207−209.
(49) Le, D.; Barinov, A.; Preciado, E.; Isarraraz, M.; Tanabe, I.; Komesu, T.; Troha, C.; Bartels, L.; Rahman, T. S.; Dowben, P. A. Spin−Orbit Coupling in the Band Structure of Monolayer WSe 2. *J. Phys. Condens. Matter* **2015**, *27*, 182201.
(50) Guan, Y.; Li, X.; Niu, R.; Zhang, N.; Hu, T.; Zhang, L. Tunable Electronic Properties of Type-Ii Sis2/Wse2 Hetero-Bilayers. *Nanomaterials* **2020**, *10*, 2037.
(51) Osada, K.; Tanaka, M.; Ohno, S.; Suzuki, T. Photoinduced Charge Transfer from Vacuum-Deposited Molecules to Single-Layer Transition Metal Dichalcogenides. *Jpn. J. Appl. Phys.* **2016**, *55*, 065201.
(52) Crispin, X.; Geskin, V.; Crispin, A.; Cornil, J.; Lazzaroni, R.; Salaneck, W. R.; Brédas, J.-L. Characterization of the Interface Dipole at Organic/ Metal Interfaces. *J. Am. Chem. Soc.* **2002**, *124*, 8131−8141.
(53) Avilov, I.; Geskin, V.; Cornil, J. Quantum-Chemical Characterization of the Origin of Dipole Formation at Molecular Organic/Organic Interfaces. *Adv. Funct. Mater.* **2009**, *19*, 624−633.
(54) Li, J.; Slassi, A.; Han, X.; Cornil, D.; Ha-Thi, M.; Pino, T.; Debecker, D. P.; Colbeau-Justin, C.; Arbiol, J.; Cornil, J.; Ghazzal, M. N. Tuning the Electronic Bandgap of Graphdiyne by H-Substitution to Promote Interfacial Charge Carrier Separation for Enhanced Photocatalytic Hydrogen Production. *Adv. Funct. Mater.* **2021**, *31*, 2100994.
(55) Slassi, A.; Gali, S. M.; Pershin, A.; Gali, A.; Cornil, J.; Beljonne, D. Interlayer Bonding in Two-Dimensional Materials: The Special Case of SnP 3 and GeP 3. *J. Phys. Chem. Lett.* **2020**, *11*, 4503−4510.
(56) Kang, J.; Liu, W.; Sarkar, D.; Jena, D.; Banerjee, K. Computational Study of Metal Contacts to Monolayer Transition-Metal Dichalcogenide Semiconductors. *Phys. Rev. X* **2014**, *4*, 031005.
(57) Muccioli, L.; D'Avino, G.; Zannoni, C. Simulation of Vapor-Phase Deposition and Growth of a Pentacene Thin Film on C 60 (001). *Adv. Mater.* **2011**, *23*, 4532.
(58) Cornil, D.; Olivier, Y.; Geskin, V.; Cornil, J. Depolarization Effects in Self-Assembled Monolayers: A Quantum-Chemical Insight. *Adv. Funct. Mater.* **2007**, *17*, 1143−1148.
(59) Coletti, C.; Riedl, C.; Lee, D. S.; Krauss, B.; Patthey, L.; von Klitzing, K.; Smet, J. H.; Starke, U. Charge Neutrality and Band-Gap Tuning of Epitaxial Graphene on SiC by Molecular Doping. *Phys. Rev. B: Condens. Matter Mater. Phys.* **2010**, *81*, 235401.
(60) Cochrane, K. A.; Zhang, T.; Kozhakhmetov, A.; Lee, J.-H.; Zhang, F.; Dong, C.; Neaton, J. B.; Robinson, J. A.; Terrones, M.; Bargioni, A. W.; Schuler, B. Intentional Carbon Doping Reveals CH as an Abundant Charged Impurity in Nominally Undoped Synthetic WS_2 and WSe_2. *2D Mater.* **2020**, *7*, 031003.

https://doi.org/10.1021/acsaelm.2c01718
ACS Appl. Electron. Mater. 2023, 5, 1660−1669